Viscoelastic properties of actin-coated membranes

E. Helfer,[1] S. Harlepp,[1] L. Bourdieu,[1,*] J. Robert,[1] F. C. MacKintosh[2] and D. Chatenay[1]
[1]*Laboratoire de Dynamique des Fluides Complexes, U.M.R. 7506, 3 rue de l'Université, 67084 Strasbourg Cedex, France*
[2]*Department of Physics, University of Michigan, Ann Arbor, Michigan 48109-1120*
(Received 1 August 2000; published 19 January 2001)

In living cells, cytoskeletal filaments interact with the plasma membrane to form structures that play a key role in cell shape and mechanical properties. To study the interaction between these basic components, we designed an *in vitro* self-assembled network of actin filaments attached to the outer surface of giant unilamellar vesicles. Optical tweezers and single-particle tracking experiments are used to study the rich dynamics of these actin-coated membranes (ACM). We show that microrheology studies can be carried out on such an individual microscopic object. The principle of the experiment consists in measuring the thermally excited position fluctuations of a probe bead attached biochemically to the membrane. We propose a model that relates the power spectrum of these thermal fluctuations to the viscoelastic properties of the membrane. The presence of the actin network modifies strongly the membrane dynamics with respect to a fluid, lipid bilayer one. It induces first a finite ($\omega=0$) two-dimensional (2D) shear modulus $G^0_{2D}\sim 0.5$ to 5 μN/m in the membrane plane. Moreover, the frequency dependence at high frequency of the shear modulus $[G'_{2D}(f)\sim f^{0.85\pm0.07}]$ and of the bending modulus $(\kappa_{ACM}(f)\sim f^{0.55\pm0.21})$ demonstrate the viscoelastic behavior of the composite membrane. These results are consistent with a common exponent of 0.75 for both moduli as expected from our model and from prior measurements on actin solutions.

DOI: 10.1103/PhysRevE.63.021904 PACS number(s): 87.19.Tt, 68.03.−g, 82.65.+r, 87.80.−y

I. INTRODUCTION

In plant and animal cells, membranes and cytoskeletal filaments interact strongly together and with other associated proteins to form stable or dynamic structures involved in cell shape, mechanical properties, and locomotion [1]. *In vitro* experiments are used to understand the interactions of these basic components of living cells and their self-assembling abilities. For example, microtubules and motors self-assemble *in vitro* into structures as asters similar to the one observed *in vivo* [2]; microtubules, polymerizing inside vesicles, can deform them far from their equilibrium shape [3]; actin filaments form cortical-like structures while growing inside vesicles [4].

Cytoskeletal filaments are biopolymers that interact with numerous proteins to achieve complex functions in cells. Another important property is their large persistence length (17 μm for actin filaments [5,6], a few millimeters for microtubules [6]) compared to the flexible polymers' one: they are thus called semiflexible polymers. This feature is at the basis of the mechanical and rheological properties of actin filaments solutions. Microrheology experiments on actin filaments in bulk have shown a frequency dependence of the elastic and loss moduli [7–9] in agreement with theoretical expectations [10]. The moduli G'_{3D} and G''_{3D} increase at high frequencies as $f^{0.75}$. Below frequencies of order 1 Hz, G'_{3D} tends towards a nearly constant (plateau) value [9,11,12].

Less is known about the mechanical properties of cytoskeletal filament and lipid membranes assemblies. Such composite structures are often observed *in vivo*, as, e.g., in the case of actin cortical networks attached to the internal leaflet of the plasma membrane [1], of spectrin networks recently observed in the Golgi apparatus [13], or of the red blood cell membrane [1]. This latter one consists of a two-dimensional (2D) network of spectrin tetramers linked together by short actin filaments and attached to the membrane by protein complexes. Whereas pure fluid lipids membranes have no shear modulus and are characterized only by their Helfrich bending elasticity [14,15] (bending modulus $\kappa_{fluid}\sim 10-20k_BT$ [15–17]), the red blood cell membrane possesses a finite shear modulus of a few μN/m [18–20] and a bending modulus of the order of 5 to $175k_BT$, depending on the measurement techniques [21–23].

This example demonstrates that networks of stiff filaments attached to lipid membranes induce strong modifications of their mechanical properties. To understand qualitatively and quantitatively how cytoskeletal networks modify the mechanical properties of membranes, we tailored composite structures obtained by self-assembly of actin filaments, stabilized in length, reticulated and biochemically attached to the surface of giant vesicles. A quasi-two-dimensional cross-linked network is formed. This tailored microstructure is composed of two components that have been widely studied in the past in isolation [5–11,14–17,24]. Besides an increase of the elastic moduli with respect to a fluid lipid membrane, a more complex dynamics is expected: we have shown recently that this system exhibits viscoelasticity [25]. We present in this paper a complete description of our experiments as well as the results demonstrating the rich dynamics of these composite membranes.

To observe and measure these dynamical properties, we perform microrheology experiments on single vesicles, using micrometer probe beads biochemically linked to the membranes. We manipulate and track the motion of these beads with optical tweezers. Our results are compared to those obtained with fluid vesicles, without the actin shell. The thermally excited position fluctuations of the beads are measured

*Author to whom correspondence should be addressed.

over a large frequency range (10 Hz up to a few kHz) with nanometer scale resolution using a position detection setup. The basic principle of the measurement is illustrated by the following simple example. For a bead trapped in solution, the power spectrum of its thermally excited position fluctuations is a Lorentzian of parameters determined only by the trap stiffness k and the drag coefficient $\zeta = 6\pi\eta R_b$ of the bead (radius R_b) in the solvent of shear viscosity η [26],

$$S(f) = \langle x^2(f) \rangle = \frac{2\zeta k_B T}{4\pi^2 \zeta^2 f^2 + k^2}. \quad (1)$$

When the bead is attached to a vesicle, the power spectrum is modified due to the forces exerted by the membrane on the bead. The membrane energy consists of a sum of a bending term (with modulus κ) [14,15] and, only in the case of actin-coated membranes, a term related to the in-plane viscoelasticity (2D complex modulus $G_{2D} = G'_{2D} + iG''_{2D}$). In this case, the power spectrum depends on k, η, κ, and G_{2D}. Therefore, changes in the spectrum before and after attachment to a vesicle are directly associated with the membrane mechanical properties. Whereas the motion of large beads is dominated by the bulk viscous drag, we show that, for small enough beads, the fluctuations in the plane of the membrane are related to its in-plane shear viscoelasticity (''in-plane'' fluctuations) and those perpendicular to the membrane plane, called ''undulations,'' to its bending elasticity (''out-of-plane'' fluctuations). We obtain by this technique a complete description of the mechanical properties of the membrane over a large frequency range.

II. MATERIALS AND METHODS

A. Biotinylated vesicles

Vesicles are composed of a mixture of two phospholipids (purchased from Avanti Polar Lipids): 1,2-Dioleoyl-sn-Glycero-3-Phosphocholine (DOPC) and 1,2-Dioleoyl-sn-Glycero-3-Phosphoethanolamine-*N*-(CapBiotinyl) (DOPE-B-Cap) which has a biotin group attached to its hydrophilic head. Both lipids have unsaturated fatty chains of 18 carbons, whose fusion temperature is below 20 °C ($T_f \sim -10$ °C) [27]. Vesicles are prepared by electroformation [28]. A solution of phospholipids, containing 95% DOPC and 5% DOPE-B-Cap dissolved in chloroform, is spread on two indium tin oxide (ITO) glass slides and dried under vacuum. The slides are assembled face to face and held apart with a Teflon spacer (1 mm thick). The swelling solution (100 mM sucrose, 2 mM Tris-HCl, pH 8.0, and 0.01% NaN_3) is injected in the chamber held at 30 °C. An alternating field of 1 Vpp and 10 Hz is applied between the two slides during 4 h. After swelling, the vesicles are diluted in a glucose solution (105 mM glucose, 2 mM Tris-HCl, pH 8.0, and 0.01% NaN_3) of same osmolarity as the sucrose one. Vesicles are then stored under argon atmosphere at 4 °C during at most two weeks. Vesicles grown by this technique are giant (up to about 50–100 μm in diameter) and known to be mostly unilamellar [29]. By labeling the biotinylated vesicles with rhodamin-streptavidin (Molecular Probes), we observe a homogeneous fluorescent contour of the vesicles (images not shown), which indicates that there is no large scale segregation between the two phospholipids.

B. Biotinylated actin filaments

Actin filaments are prepared by the standard method of Pardee and Spudich [30]. Monomeric actin is purified from acetone powder, which has been extracted from chicken muscle, and dissolved at 1.5 mg/ml in a low salt buffer (G buffer: 2 mM Tris-HCl, pH 8.0, 0.5 mM ATP (Adenosine 5′-triphosphate), 0.2 mM $CaCl_2$, 0.5 mM β-mercaptoethanol and 0.01% NaN_3). Acetone powder is kept at −30 °C and actin monomers can be stored in liquid nitrogen for at least one year. About 15% of the monomers are labeled with biotin-iodoacetamide (Molecular Probes). Actin polymerization is induced by adding 50 mM KCl and increasing the ATP concentration to 1 mM (F buffer) at an actin concentration of 0.1 mg/ml (~2.4 μM). The actin filaments are stabilized against depolymerization and fluorescently labeled with rhodamin-phalloidin (Molecular Probes) at 1 μM and stored at 4 °C for one week. The filaments are observed in fluorescence microscopy (actin concentration of 10 to 15 nM): the filaments' length lies from 1 μm to about 20 μm and the average length is of the order of 10 μm.

C. Actin-coated membranes (ACM)

Actin-coated vesicles are obtained by mixing vesicles and actin filaments in presence of streptavidin (Molecular Probes). This protein has four sites with high affinity for biotin (in saline solution) [31] and stable biochemical links are expected to establish between biotinylated lipids and actin monomers as well as between monomers themselves. Vesicles and filaments are diluted in a buffer containing 55 mM KCl, which induces also a 10% osmolarity difference between the inside and the outside of the vesicles. The osmotic pressure difference makes the fluid (uncoated) vesicles flaccid: thermal undulations of the membranes are clearly seen by videomicroscopy [17,21]. Using an actin concentration of 15 nM, a streptavidin concentration of 0.02 nM and a low concentration of vesicles (a few vesicles in the field of view of 100 μm), vesicles covered by a network of fluorescent actin filaments are obtained after about 1 h incubation (Fig. 1). In the median plane, a thin and homogeneous actin ring is visualized whereas images taken on the top or bottom of vesicles show sometimes individual filaments. Streptavidin concentration was chosen to optimize the actin density on the vesicles. Higher actin concentrations were not used since they lead to the formation of a thicker 3D gel.

The structural parameters of actin networks cannot be precisely determined from fluorescence images and may also depend significantly on the vesicles. Nevertheless, we estimate that the actin shell thickness h is below 1 μm and that the mesh size ξ of the network should also lie around 0.1 to 1 μm. Finally, it is not possible to estimate the reticulation rate of the actin gels on the vesicles; let us only note that streptavidin is a much less concentrated on the vesicle surface than actin.

Two qualitative observations demonstrate the striking effects of the actin network on the membranes properties. The

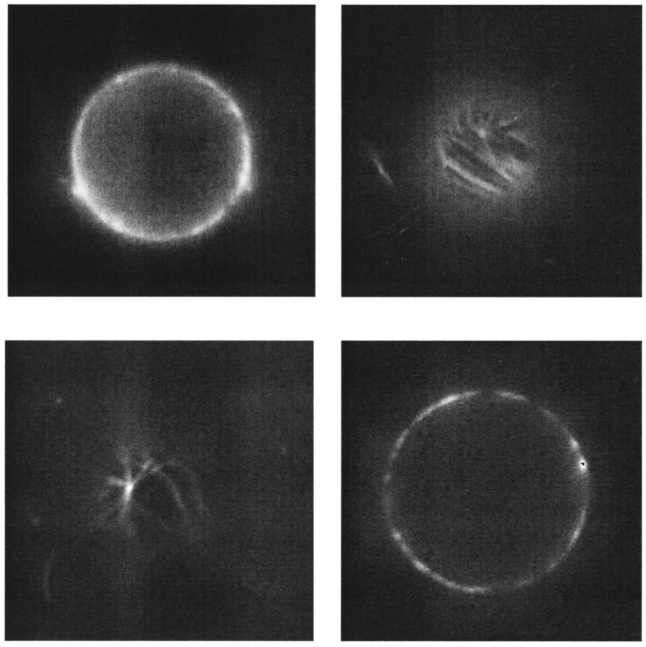

FIG. 1. Actin-coated vesicles (15 μm in diameter) observed at different planes by fluorescence microscopy. The medium planes show high fluorescent contours of the vesicles, indicating that they are homogeneously coated by an actin filaments shell. In inferior or superior planes one can sometimes distinguish individual filaments.

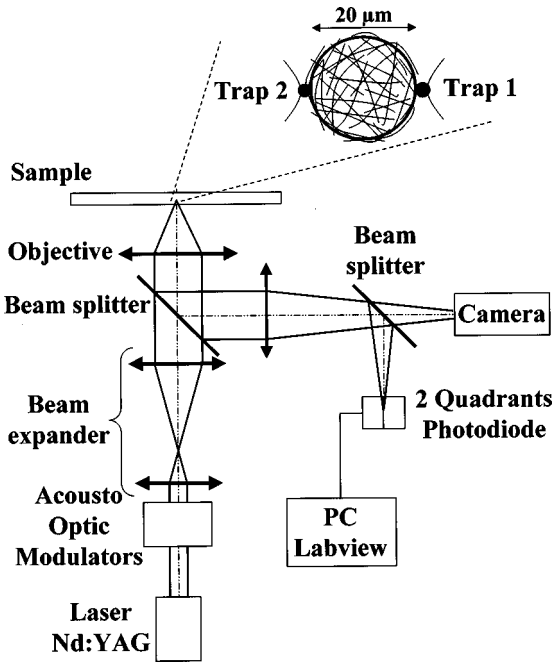

FIG. 2. The experimental setup is performed on a home-built microscope. The infrared laser (Topaz 1064 nm, Spectra Physics) is focused by the microscope objective of high numerical aperture (Plan Neofluar 100×, N.A. 1.3, Zeiss) which creates an optical trap in the objective focal plane. The rapid deflection of the laser by the acousto-optic modulators (AA.DTS.XY-250, A&A Opto-Electronique) allows us to locate one or two traps in the sample. The infrared light backscattered by the trapped bead is used to make an image of the bead on a two-quadrant photodiode (S3096-02, Hamamatsu). The difference between the two tensions (converted from the currents through 10 kΩ resistances) is amplified by a low-noise amplifier (SR-560, Stanford Research Systems) with a 30 kHz bandwidth. The differential voltage is acquired with a Lab-PC 1200 acquisition board at 60 kHz and the power spectrum of the position fluctuations is computed using a software written under Labview (National Instruments).

first of these is a considerable decrease of the thermal undulations of the vesicles contour, which can be interpreted as a significant increase of the bending modulus. Second, when two beads are attached on a vesicle (see below), a displacement tangent to the membrane plane of one of them (imposed with an optical tweezers) induces a symmetric motion of the second one. This indicates that the composite membrane has a shear modulus.

These self-assembled membranes are different from structures designed by other groups, such as actin filaments adsorbed on positively charged vesicles [32] or actin filaments growing inside vesicles and deforming them [4]. In particular, in comparison to this latter case, the actin network is in our construct intrinsically coupled to the lipid membrane by the biotin-streptavidin bonds.

D. Micromanipulation and single-particle tracking

In the case of simple fluid membranes, thermal undulations have an amplitude of the order of a few 100 nm and can be measured by videomicroscopy [17]. In contrast, in the presence of the actin network, thermal undulations are hardly visible. To measure them as well as fluctuations in the membrane plane, we have used a single-particle tracking method. Single-particle tracking techniques have been used to measure the viscoelastic properties of homogenous solutions with a high spatial accuracy and over a large frequency range [7].

Beads coated with streptavidin are mixed with vesicles just before the experiment. They can bind either to the biotinylated phospholipids (in the case of fluid vesicles) or to the biotinylated actin monomers in the filaments (actin-coated vesicles). Vesicles are studied in a closed chamber (1 mm thick) sealed with two glass coverslips coated with Bovin Serum Albumin to reduce the sticking of vesicles and actin to the glass. A probe bead held by optical tweezers is bound to a vesicle (15 to 20 μm in diameter) by moving the microscope stage. Binding occurs in a few seconds. Actin-coated vesicles attach weakly to the coverslips, which prevents large scale motion of the vesicles. In the case of fluid vesicles, a second bead (manipulated with a second optical trap) is attached to the vesicle at a position diametrically opposed to the first one and is strongly trapped to avoid vesicle displacement. The position in time of the probe bead is measured in order to compare the power spectra of the thermally excited position fluctuations of the bead before and after attachment, at several laser powers.

The setup of optical tweezers and particle position detection is implemented on a home-built microscope (Fig. 2). An infrared laser beam is highly focused by a high numerical aperture objective to trap dielectric particles. The optical trap can be displaced in the focal plane of the objective by deflecting the laser with acousto-optic modulators. Rapid

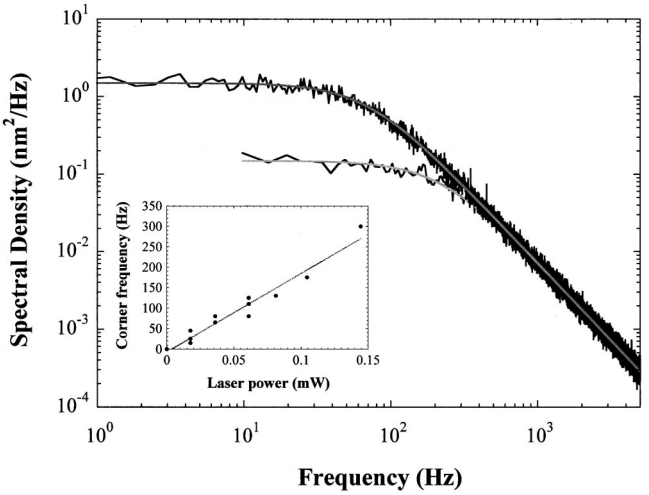

FIG. 3. Power spectra of the position fluctuations of 2.8 μm beads trapped at two different laser powers. The curve with the highest plateau value corresponds to the lowest stiffness $k = 1.1\times10^{-5}$ N/m ($f_c \sim 70$ Hz); the second one corresponds to $k = 3.7\times10^{-5}$ N/m ($f_c \sim 200$ Hz). We show in the inset the dependence of the corner frequency f_c as a function of the laser power P for 1 μm beads.

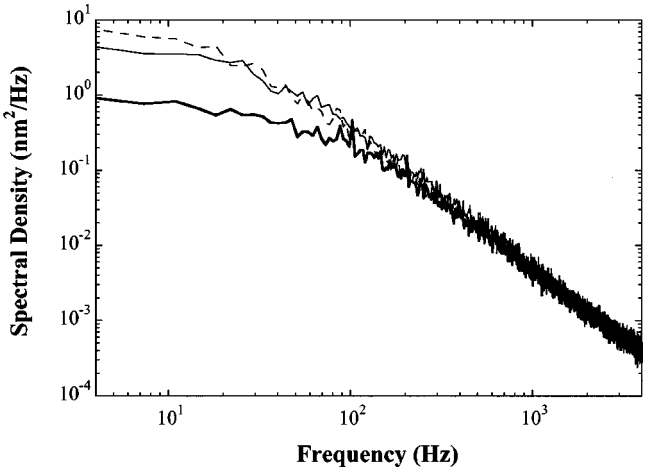

FIG. 4. Power spectra of the out-of-plane position fluctuations of a 1 μm bead attached to an actin-coated vesicle (14 μm) and trapped at different stiffnesses k of 2.5, 6.5, and 9.4 μN/m, respectively, drawn as a dashed, thin solid, and thick solid lines. Above around 200 Hz (highest corner frequency) the three curves join and a power law of exponent -1.83 ± 0.04 is fitted to the data (the error bar is statistically estimated with the three curves).

switching of the trap between different positions allows us to create multiple tweezers [33] when needed, i.e., in the case of fluid vesicles only: in order to trap two beads, the laser beam is moved every 200 μs from one location to the other one.

The infrared light backscattered by the trapped bead is used to form an image of the bead on a two-quadrant photodetector. Each quadrant delivers a current proportional to the received light intensity. The currents are converted into voltages, and their difference, amplified by a low noise amplifier, is proportional to the bead position in the trap. The bead position can be then measured with a high frequency bandwidth (up to a few kHz), once the calibration factor a (a relation between measured voltage and actual position) is determined. Depending on the orientation of the photodiode, position fluctuations parallel or perpendicular to the membrane plane are measured.

E. Principle of calibration and measurement

From the Langevin equation of the motion $x(t)$ of a bead of radius R_b in the harmonic potential of the optical tweezers, one deduces the power spectrum of the position fluctuations of the trapped bead $\langle x^2(f)\rangle$ [26] which is a Lorentzian [see Eq. (1)]. The corner frequency $f_c = k/(2\pi\zeta)$ of the spectrum depends on the trap stiffness which varies linearly with the laser power. Below f_c, the power spectrum is constant (equal to a plateau value $S_0 = 2\zeta k_B T/k^2$). Above f_c, the spectral density of the position fluctuations is that of a Brownian particle ($\sim f^{-2}$). Both the spring constant of the trap k (N/m), and the calibration factor of the tracking setup a (V/nm), are independently determined from the power spectrum of the bead motion [26]. In Fig. 3 are shown the power spectra of two beads of same size (2.8 μm in diameter) trapped with two different stiffnesses. By applying a Lorentzian fit to the data, k and a are determined in each case. The corner frequency increases as expected with the stiffness: in the inset in Fig. 3 is shown the linear dependence of f_c as a function of the laser power, in the case of 1 μm beads. The high frequency regime does not depend on the presence of the tweezers and a power law of exponent -2 ± 0.02, consistent with Brownian motion, is fitted to the data above f_c.

Once the calibration spectrum of the position fluctuations of the probe bead has been obtained, the bead is bound to the membrane (fluid or actin-coated one) and the spectrum is again computed. The bead motion is measured in two directions, perpendicular to the membrane plane (''out of plane'') and parallel to the membrane plane (''in plane''). As the fluctuations are of small amplitude, out-of-plane motion will be related to the membrane bending elasticity and in-plane displacement to its shear elasticity. In practice we use a trap stiffness as low as possible ($f_c \sim 10$ to 50 Hz): above f_c the power spectrum does not depend on k but only on the membrane properties and on the solvent viscosity. Figure 4 shows effectively that the fluctuations power spectra of a bead attached to an actin-coated vesicle are independent of the trap stiffness above the highest corner frequency.

Spectra before and after attachment to the vesicles are compared. In particular, the spectrum amplitude and the power law fitted to the data are analyzed. Power laws are fitted to the experimental spectra between 50–100 Hz (imposed by f_c) and about 1 kHz in the case of fluid membranes and 4 kHz for actin-coated ones. The limit of 1 kHz is imposed by the time sharing of the laser between two locations in the case of fluid vesicles. The second limit corresponds to an unexplained and rapid crossover in the fluctuations power spectrum of a trapped bead towards a new regime ($\sim f^{-2.5}$), which limits the frequency range well above the noise level [7]. Power spectra are therefore studied over a

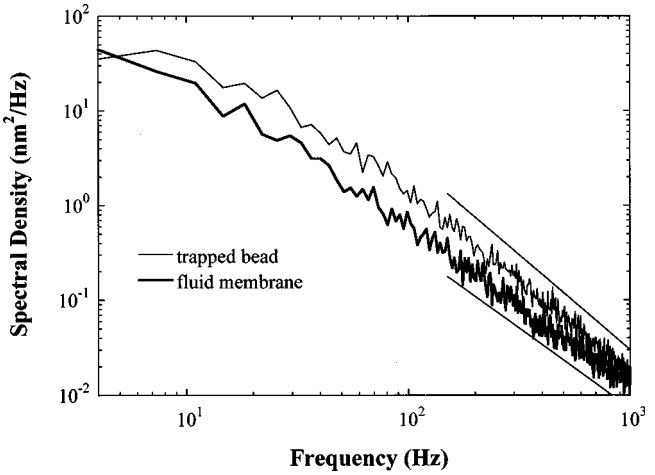

FIG. 5. Power spectrum of the out-of-plane fluctuations (thick solid line) of a 1.5 μm bead attached to a fluid vesicle (18 μm) and trapped with a small stiffness ($k=2\times10^{-6}$ N/m). It is compared to the calibration power spectrum measured for the same bead trapped in solution with the same stiffness (thin solid line). Above the trap corner frequency ($\sim$20 Hz), power laws of exponents -1.68 ± 0.03 (fluid membrane) and -2.01 ± 0.02 (trapped bead) are best fits to these data. Lines of slopes -1.68 and -2 are drawn as guides to the eyes, respectively, below and above the curves.

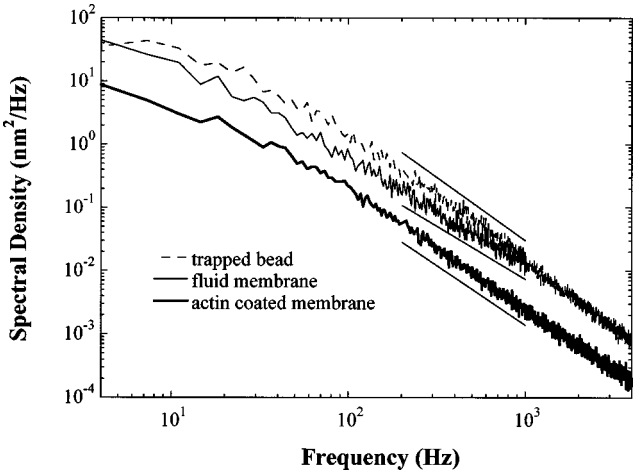

FIG. 6. Power spectra of the out-of-plane fluctuations of 1.5 μm beads trapped in solution (dashed line), attached to a fluid membrane (thin solid line) and attached to an actin-coated membrane (thick solid line). A power law of exponent -1.88 ± 0.01 best fits the last curve. Lines of slopes -2, -1.68, and -1.88 are drawn as guides to the eyes, from the top to the bottom of the picture.

frequency range of one to two decades, which corresponds to two to four decades in amplitude, making it possible to distinguish between quite close power-law exponents. Let us note that an error bar on the power-law exponent is computed for each spectrum using a least-square-fit method (the Levenberg-Marquardt algorithm). This error is mentioned in the captions of figures showing individual spectra. It is, nevertheless, smaller than the statistical error obtained from the study of a few tens of vesicles. This statistical error is used in the text.

III. RESULTS

We present results obtained with beads of 1 and 1.5 μm in diameter. Out-of-plane and in-plane fluctuations are separately analyzed. In each case, the power spectra of the position fluctuations of beads bound to fluid and actin-coated membranes are shown and compared to a calibration spectrum (trapped bead).

A. Out-of-plane fluctuations

Figure 5 shows the power spectrum obtained for the out-of-plane motion of a 1.5 μm bead attached to a fluid vesicle and weakly trapped ($k=2\times10^{-6}$ N/m) and the one measured for the same bead in the trap of same stiffness before attachment. The amplitude of the spectrum is clearly smaller in the presence of the membrane. Power laws are fitted to the data above the trap corner frequency. We measure for those two curves two different exponents of -1.68 ± 0.03 (out-of-plane power spectrum) and -2.01 ± 0.02 (calibration spectrum). In all the experiments achieved with fluid membranes, the same spectrum amplitude is measured. The average power-law exponents measured statistically are -1.7 ± 0.05 (fluid vesicle) and -2 ± 0.02 (trapped bead). The error bar of 0.05 (which is indeed larger than the individual error measured for each spectrum) is statistically estimated from 12 curves obtained with 4 vesicles and 1 or 1.5 μm beads.

In the case of actin-coated membranes, a larger decrease of the power spectrum amplitude is observed: we show in Fig. 6 the two previous spectra and the one obtained for a 1.5 μm bead attached to an actin-coated vesicle and trapped with the same stiffness. The out-of-plane power spectrum amplitude drops by a factor 3.6 (measured at 500 Hz) between the cases of the fluid membrane and of the actin-coated one. For the composite membrane, the power-law exponent is -1.88 ± 0.01. Considering all the experiments with actin-coated vesicles (24 curves and 11 vesicles), we measured first that the amplitude decreases by a factor 3 ± 1 in comparison to the fluid case (at 500 Hz). The power-law exponent fitted to the data is statistically -1.85 ± 0.07 and is different from the one obtained with fluid vesicles (-1.7 ± 0.05). Note that these close exponents can be distinguished since power laws are measured over a frequency range of 1 to 2 decades, corresponding to 2 to 4 decades in amplitude.

B. In-plane fluctuations

We show in Fig. 7 the power spectra of the in-plane fluctuations of 1 μm beads attached to a fluid and to an actin-coated vesicle in comparison to the one measured for a weakly trapped bead. One notes immediately that the presence of the fluid membrane does not affect the motion of the trapped bead. By fitting power laws to these data, we obtain similar exponents of -1.98 ± 0.02 (bead attached to the fluid membrane) and -1.97 ± 0.02 (trapped bead). This result was observed for all in-plane measurements performed with fluid membranes.

In the presence of the actin network, the power spectrum is clearly shifted towards smaller amplitude, by a factor 2 at

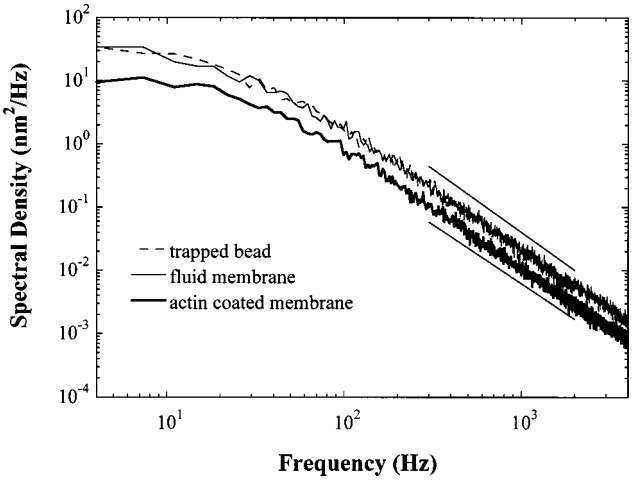

FIG. 7. Power spectra of the in-plane fluctuations of 1 μm beads trapped in solution (dashed line), attached to a fluid membrane (thin solid line), and attached to an actin-coated membrane (thick solid line). The data are best fitted by power laws of respective exponents -1.97 ± 0.02, -1.98 ± 0.02, and -1.87 ± 0.02. Lines of slopes -2 and -1.87 are, respectively, drawn above and below the curves as guides to the eyes.

500 Hz. A power law of exponent -1.87 ± 0.02 is best fitted to the curve. In all the measurements with actin-coated vesicles (18 curves and 8 vesicles), the amplitude of the in-plane power spectrum can vary by a factor of 2.5 ± 0.5, depending on the vesicle. Finally, an exponent of -1.85 ± 0.07 is measured.

IV. MODEL

We present in this section a model whose aim is to explain the variation of amplitudes and of power-law exponents observed in the previous experiments. For fluid vesicles, the energy is solely characterized by bending [14,15] (bending modulus $\kappa_{\rm fluid}\sim10-20k_BT$ [15–17]). There is no shear modulus in this case and membrane shear viscosities η_s are typically of the order of 10^{-10} to a few 10^{-9} Pa m s [34,35]. In presence of the actin network, we describe the membrane as a homogeneous medium whose energy is the sum of two terms: A bending term, as in the fluid case, but with a different bending modulus $\kappa_{\rm ACM}$, and a term related to in-plane viscoelasticity (viscoelastic complex modulus $G_{2D}=G'_{2D}+iG''_{2D}$). Moreover, we assume that the moduli G'_{2D} and G''_{2D} scale with frequency

$$G'_{2D}(f)\sim G''_{2D}(f)\sim f^z, \tag{2}$$

as in the case for bulk actin solutions ($G'_{3D}\sim G''_{3D}\sim f^z$, with $z\approx0.75$) [7–10]. This scaling is related to the semiflexible character of the actin filaments and to the relaxation of bending modes along them [10,36]. At low frequency, we assume that G'_{2D} tends towards a plateau value G^0_{2D}.

On the other hand, for a homogeneous plate of thickness h, the elastic shear (G') and bending (κ) moduli are related by a simple geometric law [37,38]:

$$\kappa=G'h^2/3. \tag{3}$$

Therefore, we also assume that the bending modulus of actin-coated vesicles depends on the frequency with the same power law as G'_{2D},

$$\kappa_{\rm ACM}(f)\sim f^z. \tag{4}$$

Using this hypothesis, we compute the thermally excited position fluctuations of the probe bead on which both the membrane and the surrounding fluid exert forces. Since fluctuations are thermally excited, their amplitude is small: as a consequence, we consider that the fluctuations in the plane of the membrane and perpendicular to it are not coupled. They are related, respectively, to the in-plane viscoelasticity and to the bending elasticity. For both directions, we first compute the fluctuations power spectrum of a point on the membrane and consider then the perturbation due to the bead.

A. Out-of-plane motion

The out-of-plane fluctuations of a point on a flat and infinite membrane are first considered. As the membrane surface tension γ is negligible [15], the thermal undulations of the membrane are dominated by the Helfrich bending energy [14,15,21],

$$E_b=\tfrac{1}{2}\int\kappa[\nabla^2h(\vec{r})]^2ds, \tag{5}$$

where κ is the bending modulus, ∇^2h is the mean curvature, and $h(\boldsymbol{r})$ is the membrane transverse displacement at the coordinate $\boldsymbol{r}$ of a planar reference state. Let the spatial Fourier transformation be $h(\boldsymbol{r})=\Sigma h_q e^{i\boldsymbol{q}\cdot\boldsymbol{r}}$, where h_q is the fluctuations amplitude of a mode $\boldsymbol{q}$ in the Fourier space. One obtains

$$E_b=\tfrac{1}{2}\,\kappa L^2\sum_q q^4h_qh_{-q}, \tag{6}$$

where L^2 is the membrane area. Using the energy equipartition theorem, one deduces from Eq. (6) the fluctuations mean square amplitude of the mode $\boldsymbol{q}$: $\langle|h_q|^2\rangle=k_BT/(\kappa L^2q^4)$. The corresponding relaxation frequency $f_q=\omega_q/2\pi$ comes from a hydrodynamic mode analysis: $\omega_q=\kappa q^3/(4\eta)$ [21]. This gives the time-dependent correlation function of the height fluctuations $h_q(t)$,

$$\langle h_q(t)h_{-q}(0)\rangle=\langle h_q^2\rangle e^{-\omega_qt}. \tag{7}$$

From this expression we deduce the variance of the fluctuations,

$$\langle\delta h^2(t)\rangle=2\sum_q\langle h_q^2\rangle(1-e^{-\omega_qt}). \tag{8}$$

Thus, using the time Fourier transform, one obtains

$$\langle\delta h^2(\omega)\rangle=2\sum_q\langle h_q^2\rangle\frac{\omega_q}{\omega^2+\omega_q^2}. \tag{9}$$

The out-of-plane fluctuations power spectrum of a point on the membrane is, therefore, as a function of $\omega = 2\pi f$,

$$\langle \delta h^2(\omega) \rangle = \frac{k_B T}{\kappa \pi} \int_0^{+\infty} \frac{dq}{q^3} \frac{\omega_q}{\omega^2 + \omega_q^2} = \frac{k_B T}{4\pi\eta\omega^2} \int_0^{+\infty} \frac{dq}{1 + \left(\frac{\kappa q^3}{4\eta\omega} \right)^2}. \quad (10)$$

Note that lower and upper limits of integration are in fact of the order of $q_{\min} \sim 2\pi/R_v$ and $q_{\max} \sim 2\pi/R_b$, where R_v and R_b are, respectively, the vesicle and the bead radii. The asymptotic result for large R_v and small R_b depends on κ and on the frequency f as follows:

$$\langle \delta h^2(f) \rangle \cong \frac{k_B T}{24 \eta^{2/3} \pi^{5/3}} \kappa^{-1/3} f^{-5/3} \propto \kappa^{-1/3} f^{-5/3}. \quad (11)$$

For simple fluid membranes, this frequency dependence corresponds to the time dependence of $t^{2/3}$ [39].

Equation (11) holds, in a first approximation, as long as the velocity gradients in the fluid are negligible at the scale of the bead, i.e., as long as the undulations wavelength $\lambda = 2\pi/q$ is large compared to the bead radius R_b. In the case $R_b \gg \lambda$, the viscous drag on the probe bead dominates its motion and the force due to the membrane undulations is negligible. Therefore, above a crossover frequency f_0 (estimated from the condition $R_b \sim \lambda$), the out-of-plane power spectrum should be the one for the simple Brownian motion of the bead in the fluid

$$\langle \delta h^2(f) \rangle \cong \frac{k_B T}{16 \pi^3 \eta R_b f^2} \quad \text{for } f \gg f_0 = \frac{\kappa \pi^2}{\eta R_b^3}. \quad (12)$$

Finally let us note that, in this approach, we consider the membrane as infinite and predict only asymptotic behaviors for large vesicles and small probe beads. We used also a spherical-harmonic decomposition of the bending modes [24], which takes into account the spherical geometry of the system, to compute the exact power spectrum amplitudes. As we shall see later, most of the experimental observations can still be understood by considering infinite and flat membranes, which provide simple analytical scaling laws.

1. Fluid membranes

In Fig. 8 are shown, in the case of a fluid membrane, the frequency behaviors of the out-of-plane power spectrum as a function of the bead radius R_b and the bending modulus κ_{fluid} (independent of the frequency). At low frequencies (below f_0), we predict from Eq. (11) a frequency-dependent behavior as $f^{-5/3}$ (referred as the *bending regime*). In this regime, the amplitude is independent of the bead size. At high frequencies (above f_0), we expect a regime independent of the vesicle and scaling with the frequency as f^{-2} (referred as the *Brownian regime*). From Eq. (12), the crossover frequency f_0 depends on R_b ($f_0 \propto R_b^{-3}$) and κ_{fluid} ($f_0 \propto \kappa_{\text{fluid}}$). For a given κ_{fluid}, an increasing R_b yields a decreasing f_0: the spectrum shows the Brownian regime over a larger frequency range [Fig. 8(a)]. For a given R_b, an increase of κ_{fluid} induces an increase of f_0 and overall a drop of the power spectrum amplitude in the bending regime [Fig. 8(b)]. Let us point out the fact that, in this case, the power spectrum depends slowly on κ_{fluid} as $\kappa_{\text{fluid}}^{-1/3}$. Assuming $\kappa_{\text{fluid}} \sim 10-20 k_B T$ [15–17], f_0 is of the order of a few kHz for a 1.5 μm bead and around 30 Hz for a 6 μm bead. By varying the bead size, it is thus possible to explore both regimes.

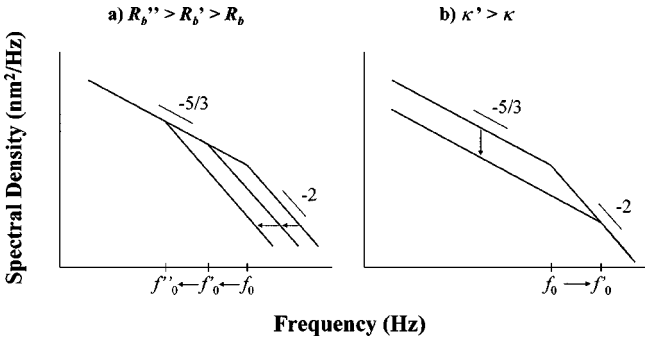

FIG. 8. Schematic dependence of the power spectrum of the out-of-plane position fluctuations in the case of a fluid membrane as a function (a) of the bead radius R_b, and (b) of the bending modulus κ_{fluid}.

2. Actin-coated membranes

We assume in this case that the bending modulus depends on the frequency as $\kappa_{\text{ACM}} \sim f^z$ [see Eq. (4)]. Thus, Eq. (11) leads to a different frequency behavior of the power spectrum of the position fluctuations (Fig. 9),

$$\langle \delta h^2(f) \rangle \propto \kappa_{\text{ACM}}^{-1/3} f^{-5/3} \propto f^{-[z/3+5/3]} \quad \text{for } f \ll f_0. \quad (13)$$

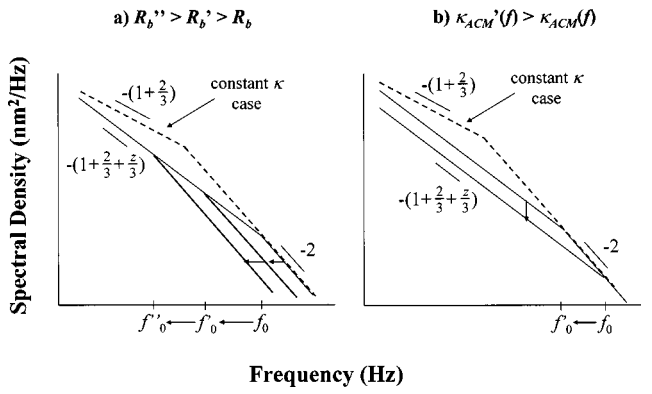

FIG. 9. Schematic dependence of the power spectrum of the out-of-plane position fluctuations in the case of an actin-coated membrane [frequency-dependent bending modulus $\kappa_{\text{ACM}}(f) \sim f^z$] as a function (a) of the bead radius R_b, and (b) of the bending modulus κ_{ACM}. Below the crossover frequency f_0, the bending regime is independent of the bead size. The power spectrum depends on the frequency as $f^{-(5+z)/3}$ and its amplitude varies as $1/[\kappa_{\text{ACM}}(f)^{1/3}]$. Above f_0, the bead motion is dominated by the fluid viscosity and the power spectrum is the one for Brownian motion ($\sim f^{-2}$). f_0 varies as $1/R_b^3$ and is proportional to $\kappa_{\text{ACM}}(f_0)$.

Therefore, the presence of the actin network has two effects. First, the amplitude of the out-of-plane power spectrum drops from the fluid case ($\langle \delta h^2 \rangle_{\text{fluid}}$) to the actin-coated case ($\langle \delta h^2 \rangle_{\text{ACM}}$),

$$\frac{\langle \delta h^2 \rangle_{\text{fluid}}}{\langle \delta h^2 \rangle_{\text{ACM}}} \approx \left(\frac{\kappa_{\text{ACM}}}{\kappa_{\text{fluid}}} \right)^{1/3}. \tag{14}$$

On the other hand, we expect different power-law exponents [$-5/3$ and $-(5/3+z/3)$] for the power spectra measured, respectively, with fluid and actin-coated vesicles. Again, Eq. (13) holds up to a frequency f_0 above which bulk viscous effects on the bead dominate. However, it is difficult to give an estimate of f_0 since, using Eq. (12), f_0 is now a solution of $f_0 = \kappa_{\text{ACM}}(f_0)\pi^2/\eta R_b^3$. Since the membrane is stiffer with increasing frequencies, the regime dominated by bulk viscosity should nevertheless happen at much higher frequencies (in comparison to the fluid case), whatever the bead size.

B. In-plane motion

1. Fluid membranes

As fluid membranes have no shear modulus, the in-plane motion of the probe beads is controlled by the viscous drags of the membrane and of the fluid. The drag coefficients related to the membrane surface viscosity η_s (10^{-10}–10^{-9} Pa m s) [34,35] and to the solvent viscosity η (10^{-3} Pa s) are, respectively, $\zeta_s = 4\pi\eta_s \sim 10^{-9}$–$10^{-8}$ Pa m s and $\zeta_v = 6\pi\eta R_b \sim 10^{-8}$ Pa m s (for a bead of 1 μm in diameter). The problem of the friction felt by a solid particle moving under gravity along a vesicle contour has been studied in detail [34]. The authors have shown that the presence of the membrane increases the effective friction on the bead (with respect to the bulk friction $6\pi\eta R_b$). When the bead remains on the outside of the vesicle (which is the case in our experiments) and for a vesicle large compared to the bead size (typically an aspect ratio larger than 7), the friction increases typically by about 25%. Therefore, we expect a power spectrum which scales as for Brownian motion at high frequency (f^{-2}) and a small amplitude decrease ($\sim$25–30%) due to an increased viscous shear.

2. Actin-coated membranes

We consider first the position fluctuations of a point on the membrane. The presence of the bead is then taken into account. Dynamical regimes distinct from those of the out-of-plane motion are expected. The membrane in-plane dynamics is related to its two-dimensional shear viscoelasticity, characterized by the complex modulus $G_{2\text{D}}(\omega) = G'_{2\text{D}}(\omega) + iG''_{2\text{D}}(\omega)$, where $G'_{2\text{D}}$ and $G''_{2\text{D}}$ are, respectively, the pulsation-dependent elastic and loss moduli. The in-plane displacement $\delta u(\omega)$ of a point on the membrane is related to a perturbative force $F(\omega)$ in the membrane plane as follows [7]:

$$\langle \delta u(\omega) \rangle = \alpha(\omega) F(\omega) \cong \frac{1}{4\pi G_{2\text{D}}(\omega)} F(\omega), \tag{15}$$

where the compliance $\alpha(\omega) = \alpha'(\omega) + i\alpha''(\omega)$ is the complex response function. Using the fluctuation-dissipation theorem, the power spectrum of the in-plane fluctuations is computed from Eq. (15) [7,40],

$$\langle \delta u^2(\omega) \rangle \cong \frac{2k_BT}{\omega} \text{Im}\left(\frac{1}{4\pi G_{2\text{D}}(\omega)} \right) = \frac{k_BT}{2\pi\omega} \frac{G''_{2\text{D}}(\omega)}{G'^2_{2\text{D}}(\omega) + G''^2_{2\text{D}}(\omega)}. \tag{16}$$

The power spectrum, as a function of the frequency $f = \omega/2\pi$, is thus

$$\langle \delta u^2(f) \rangle \cong \frac{k_BT}{4\pi^2 f} \frac{G''_{2\text{D}}(f)}{G'^2_{2\text{D}}(f) + G''^2_{2\text{D}}(f)}. \tag{17}$$

Since we assume that $G'_{2\text{D}}(f)$ and $G''_{2\text{D}}(f)$ both scale at high frequencies as f^z and knowing that $G''_{2\text{D}} = G'_{2\text{D}} \tan(\pi z/2)$ [12], the in-plane fluctuations power spectrum scales with the frequency as

$$\langle \delta u^2(f) \rangle \cong \frac{k_BT}{4\pi^2 f G''_{2\text{D}}(f)} \frac{\tan\left(\frac{\pi z}{2}\right)}{1 + \tan^2\left(\frac{\pi z}{2}\right)} \cong \frac{k_BT}{8\pi^2} \sin(\pi z) \frac{1}{f G'_{2\text{D}}(f)} \propto f^{-(1+z)}. \tag{18}$$

In the presence of the probe bead, Eq. (18) holds as long as the bulk viscous force F_v acting on the bead ($F_v \sim \zeta_v 2\pi f \delta u$) is smaller than the elastic force F_m due to the membrane [$F_m \cong 4\pi G'_{2\text{D}}(f)\delta u$], where δu is the in-plane displacement. At high frequencies, the former dominates and the bead motion is Brownian ($\langle x^2(f) \rangle \sim f^{-2}$). The crossover frequency f_1 is estimated when the two forces are of the same magnitude

$$f_1 \cong \frac{G'_{2\text{D}}(f_1)}{3\pi\eta R_b}. \tag{19}$$

At low frequencies, one predicts a regime dominated by the membrane fluctuations (referred as the *viscoelastic regime*), where the elastic shear modulus $G'_{2\text{D}}(f)$ [see Eq. (18)] can be measured. Above f_1, one reaches a Brownian regime as in the case of the out-of-plane motion. In Fig. 10 are plotted the theoretical power spectra of the bead thermally excited position fluctuations as a function of the bead size and of the zero-frequency shear modulus $G^0_{2\text{D}}$. The power spectra depend on the frequency, respectively, as $f^{-(1+z)}$ and f^{-2} below and above the crossover frequency f_1. Equation (19) shows that f_1 increases with $G^0_{2\text{D}}$: the stiffer the actin gel, the larger in frequency the viscoelastic regime. On the other hand, f_1 scales as $1/R_b$. By varying R_b, it may be thus possible to explore the different fluctuation regimes.

To estimate f_1, we first need an order of magnitude of $G^0_{2\text{D}}$. To this purpose, the actin-coated membrane is de-

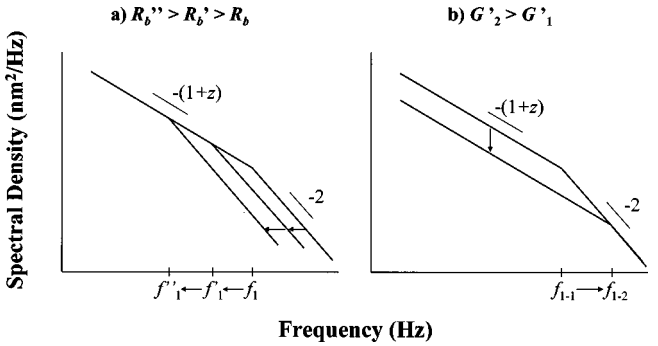

FIG. 10. Schematic dependence of the power spectrum of the in-plane position fluctuations in the case of an actin-coated membrane [frequency-dependent shear modulus $G'_{2D}(f) \sim f^z$] as a function (a) of the bead radius R_b, and (b) of the zero-frequency shear modulus G^0_{2D}. Below the crossover frequency f_1, the viscoelastic regime is independent of the bead size. The power spectrum depends on the frequency as $f^{-(1+z)}$ and its amplitude varies as $1/G'_{2D}(f)$. Above f_1, the bead motion is dominated by the fluid viscosity and the power spectrum is the one for Brownian motion ($\sim f^2$). f_1 is proportional to $1/R_b$ and to $G'_{2D}(f_1)$.

formed tangentially by moving an attached bead using an optical trap. The position of the bead is measured by videomicroscopy for different trap stiffnesses. The bead position is defined by the equilibrium between the forces exerted by the optical trap $[F_t = k(s_t - s_b)]$ and the shear force due to the membrane $(F_m \cong 4\pi G_0 s_b)$ [37,38], where k is the (varying) trap stiffness, s_t is the fixed trap position, and s_b is the bead position along the vesicle contour. Figure 11 shows that F_t is effectively a linear function of the bead position and G^0_{2D} lies between 0.5 and 5 μN/m (which is of the same order of magnitude as the shear modulus of the red blood cell membrane [18–20]). The large dispersion of the values is a consequence of the heterogeneity of the actin coating on the

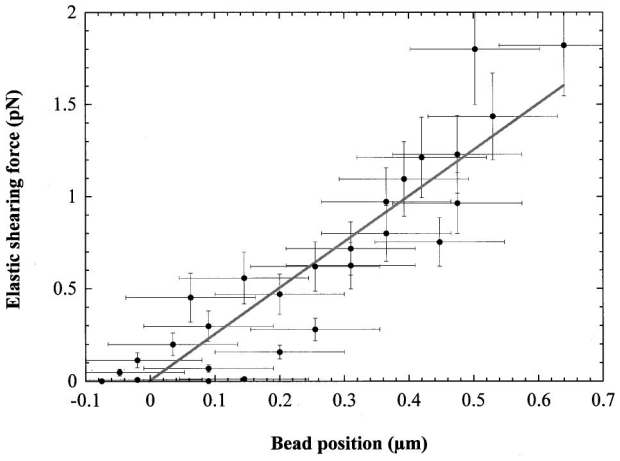

FIG. 11. Estimation of the zero-frequency shear modulus of the actin-coated membrane. A bead attached to the membrane is displaced with an optical trap along the membrane contour. The bead position is then measured as the trap stiffness is lowered. The membrane shear force is plotted as a function of the bead position. A linear fit to the data gives an estimate of the shear modulus G^0_{2D} of 8×10^{-7} N/m.

vesicles. In bulk, the plateau modulus G_p and the mesh size ξ depend on the actin concentration c as $G_p \sim c^{2.5}$ [41] and $\xi \sim c^{-0.5}$ [42], which leads to $G_p \sim \xi^{-5}$. Therefore, assuming that G^0_{2D} behaves as G_p, a small variation of ξ (by less than a factor 2, which is possible from the fluorescence microscopy images) corresponds to one magnitude order variation for G^0_{2D}. A lower estimate of f_1 is finally obtained by using $G^0_{2D}(\sim 1\ \mu\text{N/m})$ in Eq. (19): $f_1 \gg 200$ Hz, for a 1 μm bead. Therefore, the viscoelastic regime should be accessible, at least with small beads, in our experiments.

V. DISCUSSION

A. Fluid vesicles

Results obtained on fluid vesicles (Figs. 5 and 7) are in good agreement with the theory. For the in-plane direction, as we mentioned before, we do not see the effect of the membrane on the power spectra, with respect to the bulk case. This means that the shear viscous drag on the bead is of the same magnitude order as the bulk viscous drag (or at most one order smaller), as expected [34,35]: we are not sensitive with our technique (i.e., in the amplitude change) to an increase of the shear viscosity of the order of 25%. The power spectrum follows a f^{-2} power law, which indicates that the surface viscosity remains constant up to 1 kHz. This Brownian behavior is observed independent of the bead size (from 1 μm up to 6 μm in diameter), as expected from the model.

For the out-of-plane direction, the power spectra measured at high frequency with 1.5 μm beads are best fitted statistically with the exponent -1.7 ± 0.05, as mentioned before (see Fig. 5). This is in agreement both with the frequency dependence of the theoretical power spectrum ($f^{-5/3}$) and with the estimate of the crossover frequency $f_0(\sim 2$ kHz), below which the bending regime dominated by the membrane undulations can be measured. Moreover, the exact amplitude of the power spectrum is predicted in a good approximation with the spherical-harmonic model and a bending modulus $\kappa_{\text{fluid}} = 20 k_B T$. These data will be shown elsewhere.

A consequence of our model is the fact that the bending regime can only be observed with small beads since f_0 varies rapidly with R_b as predicted by Eq. (12): for 6, 3.1, and 1.5 μm beads, f_0 is expected to lie, respectively, around 30 Hz, 250 Hz, and 2 kHz using $\kappa \sim 10-20 k_B T$ [15–17]. For each of these bead sizes, the out-of-plane power spectra in the presence of the fluid membrane and in the solution are compared in Fig. 12. The two power spectra are identical in the case of the 6 μm bead ($\langle x^2(f) \rangle \sim f^{-2}$), as expected since $f_0 \sim 30$ Hz. As described above, a different regime is observed with 1.5 μm beads [$\langle x^2(f) \rangle \sim f^{-1.7}$]. With 3.1 μm beads, an intermediate situation is shown: the two spectra collapse around 600–700 Hz, which is explained by the approximative predicted value of $f_0 \sim 200$ Hz. The frequency range is nevertheless too small to demonstrate clearly the two power-law dependences in this case.

To conclude, our model is in agreement with the experiments achieved with fluid vesicles and the known mechani-

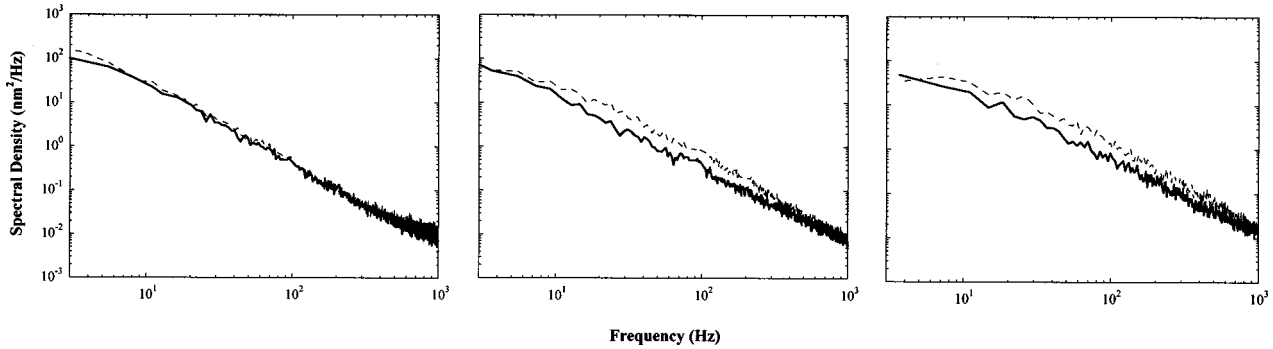

FIG. 12. Power spectra of the out-of-plane position fluctuations of beads attached to fluid vesicles as a function of the bead diameter: 6, 3.1, and 1.5 μm from left to right. In each case, the power spectrum is compared to a calibration power spectrum of the bead trapped in solution with the same trap stiffness.

cal properties of fluid lipid membranes: a bending modulus of the order of 10 to $20k_BT$, no shear elastic modulus and a shear viscous drag of the order of a few 10^{-9} Pa m s. The frequency dependence of the power spectrum in the regime dominated by the membrane bending undulations is clearly evidenced as $f^{-5/3}$.

B. Actin-coated vesicles

1. Out-of-plane fluctuations

Out-of-plane power spectra obtained with small beads (1 and 1.5 μm in diameter) show two main differences with respect to fluid membranes. As mentioned before, the amplitude of the spectra is significantly lower (by a factor 3 ± 1 at 500 Hz) and a power law of exponent -1.85 ± 0.07 best fits the data. This behavior illustrates, according to our model, the viscoelastic character of the actin-coated membrane.

The amplitude drop of the power spectrum in presence of the actin shell corresponds to an increase in the actin-coated membrane bending modulus κ_{ACM}, which can be estimated using Eq. (14) and assuming $\kappa_{\mathrm{fluid}}\sim10-20k_BT$. It lies between 100 and $1000k_BT$, depending on the vesicles. This huge increase of the bending rigidity is not only the sum of the bending stiffness of the rigid filaments on the surface. This would indeed yield typically a frequency independent bending modulus $\kappa_{\mathrm{ACM}}\sim k_BTL_ph/\xi^2$, which is at most $100k_BT$ with $L_p\sim10$ μm, $h<1$ μm, and $\xi>0.1$ μm.

Thus, the increase of the bending rigidity corresponds on the contrary to a frequency-dependent bending modulus, as proposed in our model [see Eqs. (11) and (13)]. This feature explains both the power-law dependence of the power spectra and the very large values of the bending modulus. Equation (13) leads to

$$\kappa_{\mathrm{ACM}}\sim f^z \quad \text{with} \quad z=0.55\pm0.21. \tag{20}$$

To check the validity of our model, we study the evolution of the out-of-plane power spectrum as a function of the bead size (6, 3.1, and 1.5 μm in diameter) (Fig. 13). In this case, even with large beads, we do not observe a power spectrum identical to the one measured in bulk. The power-law exponents fitted to each of these curves are close and different from -2: -1.82 ± 0.03 (6 μm bead), -1.83 ± 0.03 (3.1 μm bead), and -1.88 ± 0.01 (1.5 μm bead). The statistical study performed with these three sizes of beads leads to the conclusion that the power-law exponents cannot be distinguished and that a common power law of exponent -1.85 ± 0.07 best fits to all the data, whatever the bead size. As an example, five power spectra measured with all sizes of beads (1 to 6 μm in diameter) are shown in Fig. 14: whereas

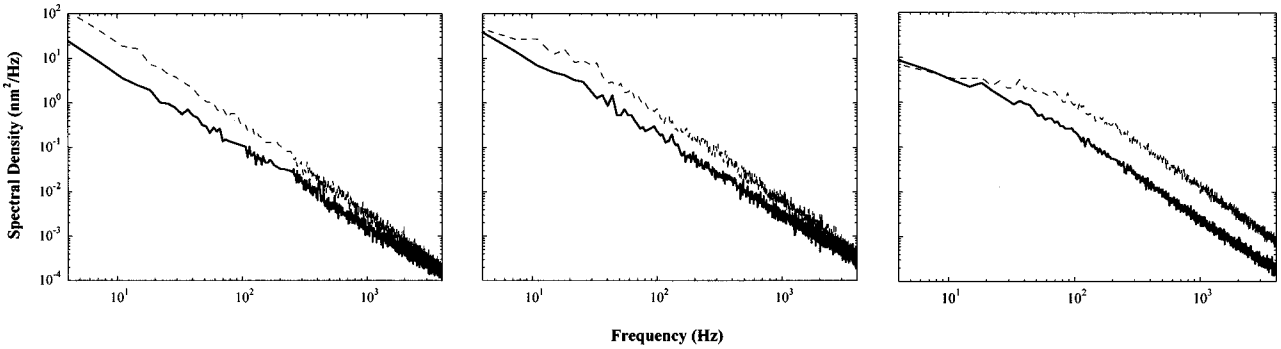

FIG. 13. Power spectra of the out-of-plane position fluctuations of beads attached to actin-coated vesicles as a function of the bead diameter: 6, 3.1, and 1.5 μm from left to right. In each case, the power spectrum is compared to a calibration spectrum of the bead trapped in solution with the same trap stiffness. Power laws of exponents, respectively, -1.82 ± 0.03, -1.83 ± 0.03, and -1.88 ± 0.01 best fit the data. These power laws are in agreement with a common exponent of -1.85 ± 0.07 obtained from a statistical study over the different bead sizes.

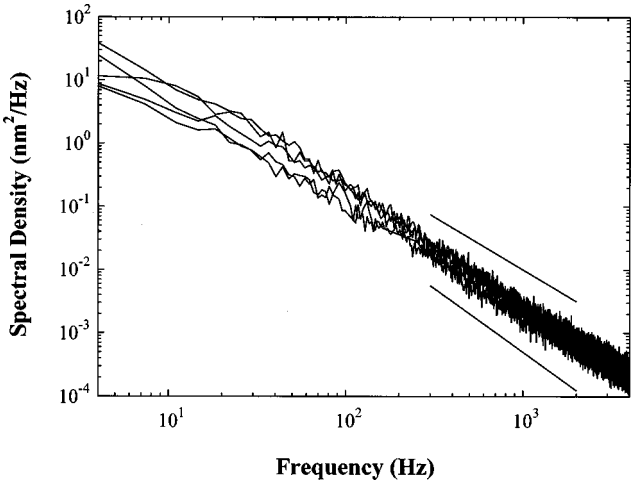

FIG. 14. Power spectra of the out-of-plane position fluctuations for actin-coated membranes obtained with bead sizes from 1 to 6 μm. Lines of slopes $-5/3$ and -2 are drawn, respectively, above and below the curves as guides to the eyes. An intermediate slope of -1.85 ± 0.05 is fitted to these five power spectra (the error bar is statistically estimated for the five curves shown here).

the amplitude of those curves varies by a factor of 2.75 ± 0.25, they follow, whatever the bead size, the same power law of exponent -1.85 ± 0.05. This means that the crossover frequency f_0 between the bending regime and the Brownian regime has increased. From Eq. (12) [$f_0\sim\kappa_{\mathrm{ACM}}(f_0)$], this result is consistent with a large increase of the bending stiffness. For example, with 6 μm beads, f_0 (estimated from the collapse of the out-of-plane spectrum and the calibration spectrum) lies around a few kHz corresponding to a consistent bending modulus of the order of $1000k_BT$ at those frequencies. The bead size evolution of the power spectra is therefore in very good agreement with our conclusion that the bending modulus is frequency dependent according to Eq. (20).

2. In-plane fluctuations

In-plane fluctuations power spectra measured with small beads (1 and 1.5 μm) for actin-coated membranes show two features in comparison to the fluid membranes case. An amplitude drop (by a factor 2.5 ± 0.5 with respect to the one of fluid membranes) and a power-law dependence (-1.85 ± 0.07) different from Brownian motion (f^{-2}). These two changes show again the viscoelasticity of the membrane. Using Eq. (18), the frequency dependence of the shear modulus is directly computed from the in-plane fluctuations power spectrum,

$$G'_{2\mathrm{D}}(f)\cong\frac{k_BT}{8\pi^2}\sin(\pi z)\,\frac{1}{f\langle\delta u^2(f)\rangle}. \tag{21}$$

The shear moduli obtained from three power spectra with amplitudes of the same magnitude order are plotted in Fig. 15. Considering all experiments with 1 and 1.5 μm beads (18 curves and 8 vesicles), we obtain that the shear modulus scales at high frequencies as

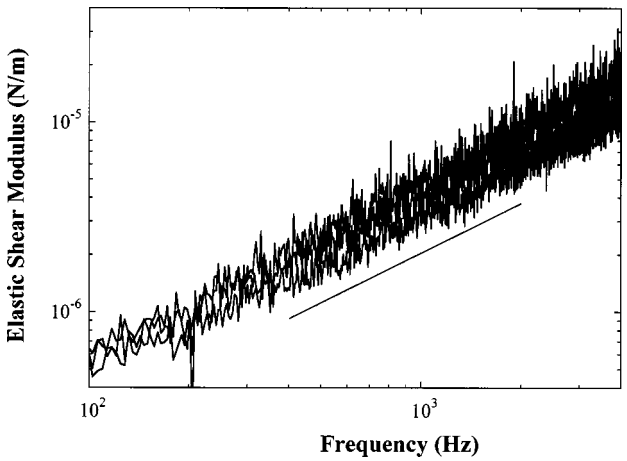

FIG. 15. Frequency dependence of the shear modulus $G'_{2\mathrm{D}}(f)$. Using Eq. (22), $G'_{2\mathrm{D}}(f)$ is deduced above the trap corner frequencies from the power spectra of in-plane fluctuations of 1 μm beads attached to three different actin-coated vesicles. $G'_{2\mathrm{D}}(f)$ scales here as $f^{0.87\pm0.02}$. A line $f^{0.87}$ is drawn as a guide to the eyes.

$$G'_{2\mathrm{D}}(f)\sim f^z \quad \text{with} \quad z=0.85\pm0.07. \tag{22}$$

This provides a self-consistent estimate of 10 kHz for the crossover frequency f_1, above which bulk viscous effects dominate [see Eq. (19)]. Moreover, the magnitude of the shear modulus determined by this method is in good agreement with the estimate of the plateau modulus obtained by micromanipulation ($G^0_{2\mathrm{D}}\sim0.5\text{–}5\times10^{-6}$ N/m). In both cases, we observe a broad range of values (Fig. 16), which we relate to the variation of the network parameters from one vesicle to the other. Nevertheless, the plateau frequency (above which the shear modulus is increasing) cannot be determined accurately here, but its value lies below 100 Hz.

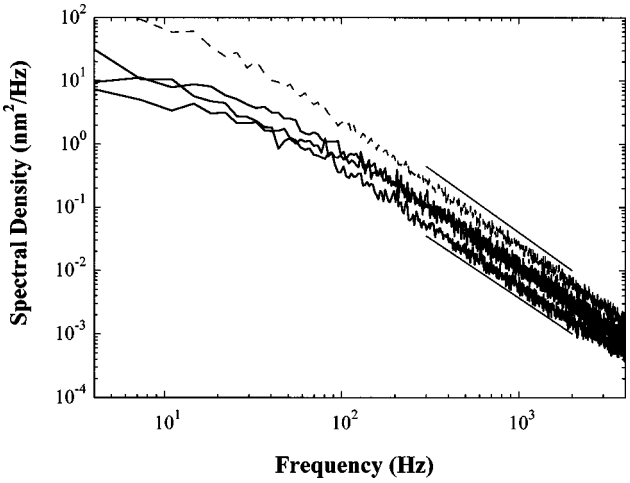

FIG. 16. Power spectra of the in-plane position fluctuations of 1 μm beads attached to actin-coated vesicles. A calibration power spectrum of a 1 μm bead trapped in the fluid (dashed line) is shown for comparison. A common power-law exponent of -1.87 ± 0.02 is measured for these three curves. Lines f^{-2} and $f^{-1.87}$ are drawn as guides to the eyes, respectively, above and below the power spectra.

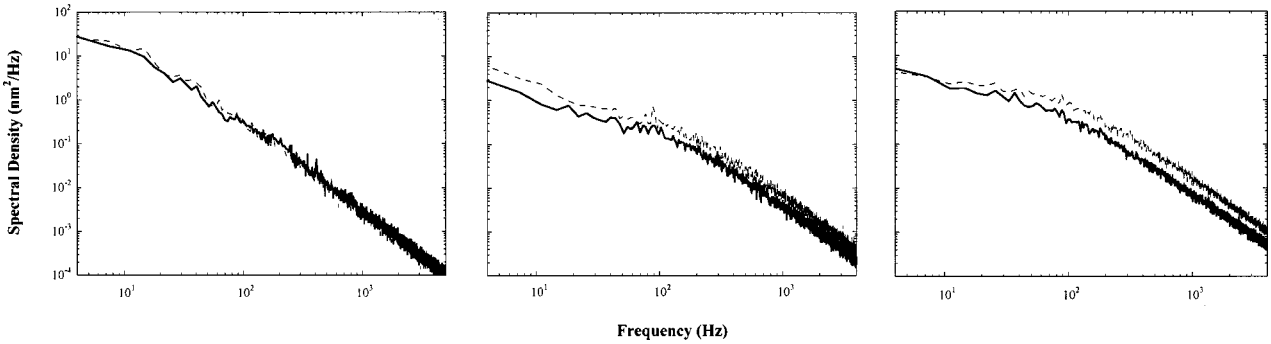

FIG. 17. Power spectra of in-plane position fluctuations of beads attached to actin-coated vesicles as a function of the bead diameter: 6, 3.1, and 1.5 μm from left to right. In each case, the power spectrum is compared to a calibration power spectrum of the bead trapped in solution with the same trap stiffness. Power laws are fitted to the data: the exponents are, respectively, -2.08 ± 0.06, -1.94 ± 0.03, and -1.87 ± 0.02.

To check if this model is valid, we also study the evolution of the in-plane power spectrum as a function of the bead radius. In Fig. 17 are shown the in-plane power spectra compared to the calibration power spectra for three bead sizes (6, 3.1, and 1.5 μm). The amplitude drop between each pair of spectra decreases with an increasing bead size. Consistently, the power-law fitted to the data varies with the bead size: we measure exponents of -2.08 ± 0.06 for the 6 μm bead and -1.94 ± 0.03 for the 3.1 μm one (data shown in Fig. 17), -1.9 for 2 μm beads (data not shown), whereas an exponent of -1.85 ± 0.07 is measured for all experiments with 1 and 1.5 μm beads. By varying the bead size, we observe, as predicted in our model, a transition between the regime where the bulk viscous drag dominates and the regime where the in-plane shear viscoelasticity governs the bead motion. To understand why this transition is smooth, the hydrodynamics around the probe bead needs to be more accurately described.

Finally, the self-assembled actin-coated membranes have the following properties. The presence of the actin network induces the onset of a finite zero-frequency shear modulus G^0_{2D} (of the order of 1 μN/m) and a strong increase of the bending modulus (a few $100k_BT$ at 500 Hz). Moreover, the membrane is viscoelastic as proved by the frequency dependence of the bending modulus and of the shear modulus:

$$\kappa_{ACM}(f)\sim f^{0.55\pm0.21} \quad \text{and} \quad G'_{2D}(f)\sim f^{0.85\pm0.07}. \quad (23)$$

These two scaling laws are not inconsistent with a common exponent of 0.75, as proposed in our model in relation to 3D bulk rheology of actin. In this approach, both moduli are related in Eq. (3) by a simple quantitative relation: $\kappa_{ACM}(f)\sim[G'_{2D}(f)h^2]/3$, with h of the order of 1 μm. This corresponds to $\kappa_{ACM}\sim100k_BT$ for $G^0_{2D}\sim1$ μN/m at zero frequency, and $\kappa_{ACM}\sim1000k_BT$ for $G'_{2D}\sim4$ μN/m at 500 Hz (see Fig. 15). The difference between the two exponents may be due, however, to a relation between κ_{ACM} and G'_{2D} more complicated than the linear one for a homogeneous plate.

VI. CONCLUSION

Whereas the elasticity of fluid membrane has been studied extensively, less is known experimentally about viscoelastic, solid, or polymerized membranes, because few examples of this has been found [43,44]. Using biomolecules that possess some original mechanical and rheological properties with respect to physico-chemical systems, we have tailored, by self-assembling membranes and cytoskeletal polymers, complexes that exhibit rich dynamical properties and, in particular, viscoelasticity.

In order to characterize the viscoelasticity of the vesicles coated with actin filaments, we developed an experiment that combines micromanipulation with optical tweezers and single-particle tracking. We show that mechanical experiments can be achieved on these micrometer-sized systems. The analysis of thermally excited position fluctuations of probe beads bound to the membranes is related to the viscoelastic behavior of these membranes.

We obtain a description of the composite membrane that is independent of its microscopic detail. The presence of the actin shell increases the bending modulus and induces the existence of a 2D shear modulus. Both moduli scale with frequency with respective power-law exponents of 0.55 ± 0.21 and 0.85 ± 0.07. These exponents are consistent with a common exponent of 0.75, which is expected from bulk actin solution rheology. Whether the cell uses these dynamical properties of similar membranes is still an open question.

ACKNOWLEDGMENTS

We thank C. Marques and T. Duke for helpful discussions. F.C.M. was supported by the CNRS, the National Science Foundation, and the Whitaker Foundation. This work was supported in part by Fondation pour la Recherche Médicale.

[1] B. Alberts *et al.*, *Molecular Biology of the Cell* (Garland, New York, 1994).
[2] F. Nédelec *et al.*, Nature (London) **389**, 305 (1997).
[3] H. Hotani and M. Miyamoto, Adv. Biophys. **26**, 135 (1990); M. Elbaum, D. K. Fygenson, and A. Libchaber, Phys. Rev. Lett. **76**, 4078 (1996); D. K. Fygenson *et al.*, Phys. Rev. E **55**, 850 (1997).
[4] J. D. Cortese *et al.*, Proc. Natl. Acad. Sci. U.S.A. **86**, 5773 (1989); H. Miyata and H. Hotani, *ibid.* **89**, 11 547 (1992); W. Häckl, M. Bärmann, and E. Sackmann, Phys. Rev. Lett. **80**, 1786 (1998).
[5] A. Ott *et al.*, Phys. Rev. E **48**, 1642 (1993).
[6] F. Gittes *et al.*, J. Cell Biol. **120**, 923 (1993).
[7] F. Gittes *et al.*, Phys. Rev. Lett. **79**, 3286 (1997); B. Schnurr *et al.*, Macromolecules **30**, 7781 (1997).
[8] A. Palmer *et al.*, Biophys. J. **76**, 1063 (1999).
[9] T. Gisler and D. A. Weitz, Phys. Rev. Lett. **82**, 1606 (1999).
[10] D. C. Morse, Phys. Rev. E **58**, 1237 (1998); F. Gittes and F. C. MacKintosh, *ibid.* **58**, 1241 (1998).
[11] R. Ruddies *et al.*, Eur. Biophys. J. **64**, 1559 (1993).
[12] M. Doi and S. F. Edwards, *The Theory of Polymer Dynamics* (Clarendon, Oxford, 1986).
[13] K. A. Beck and W. J. Nelson, Biochim. Biophys. Acta **1404**, 153 (1998).
[14] W. Helfrich, Z. Naturforsch. C **28**, 693 (1973).
[15] For a review, see U. Seifert, Adv. Phys. **46**, 13 (1997).
[16] E. A. Evans and W. Rawicz, Phys. Rev. Lett. **64**, 2094 (1990); H. P. Duwe, J. Käs, and E. Sackmann, J. Phys. (France) **51**, 945 (1990).
[17] J. F. Faucon *et al.*, J. Phys. (France) **50**, 2389 (1989).
[18] R. Waugh and E. Evans, Biophys. J. **26**, 115 (1979).
[19] R. M. Hochmuth, N. Mohandas, and P. L. Blackshear, Biophys. J. **13**, 747 (1973).
[20] S. Hénon *et al.*, Biophys. J. **76**, 1145 (1999).
[21] F. Brochard and J. F. Lennon, J. Phys. (France) **36**, 1035 (1975).
[22] H. Strey, M. Peterson, and E. Sackmann, Biophys. J. **69**, 478 (1995).
[23] E. A. Evans, Biophys. J. **43**, 27 (1983).
[24] M. B. Schneider, J. T. Jenkins, and W. W. Webb, J. Phys. (France) **45**, 1457 (1984); S. T. Milner and S. A. Safran, Phys. Rev. A **36**, 4371 (1987).
[25] E. Helfer *et al.*, Phys. Rev. Lett. **85**, 457 (2000).
[26] F. Gittes and C. F. Schmidt, Methods Cell Biol. **55**, 129 (1998).
[27] R. R. C. New, *Liposomes*, Practical Approach Series (Oxford University Press, Oxford, 1990).
[28] M. I. Angelova *et al.*, Springer Proc. Phys. **66**, 178 (1992).
[29] L. Mathivet, P. F. Devaux, and S. Cribier, Biophys. J. **70**, 1112 (1996).
[30] J. D. Pardee and J. A. Spudich, Methods Cell Biol. **24**, 271 (1982).
[31] N. M. Green, Adv. Protein Chem. **29**, 85 (1975).
[32] A. Laliberte and C. Gicquaud, J. Cell Biol. **106**, 1221 (1988).
[33] J. E. Molloy, Methods Cell Biol. **55**, 205 (1998).
[34] K. Velikov *et al.*, Europhys. Lett. **40**, 405 (1997); R. Dimova *et al.*, Eur. Phys. J. B **12**, 589 (1999); K. Velikov *et al.*, Colloids Surf. A **149**, 245 (1999).
[35] R. D. Kornberg and H. M. McConnel, Proc. Natl. Acad. Sci. U.S.A. **68**, 2564 (1971); J. F. Tocanne, L. Dupou-Cezanne, and A. Lopez, Prog. Lipid Res. **33**, 203 (1994).
[36] R. Everaers *et al.*, Phys. Rev. Lett. **82**, 3717 (1999). Here, the authors show that at short times, the dynamics differ from those shown previously in Ref. [10]. This is due to the finite speed of propagation of tension. In a time t, the tension propagates a length $l_1 \approx \sqrt{l_p l(t)}$, where l_p is the persistence length and $l(t) \approx (4\kappa t/\eta)^{1/4}$ represents the longest wavelength bending mode that can relax in time t. These authors show that for a filament segment of length L, the initial longitudinal mean-square displacement of a filament end grows with time as $\delta x^2 \approx t^{7/8}$ until l_1 exceeds L. This occurs in a time of order $(\eta L^4/\kappa)(L/l_p)^4$ which, for instance, is approximately 10^{-6} s for a segment of length 1 μm.
[37] L. Landau and E. Lifchitz, *Théorie de l'élasticité* (Mir, Moscow, 1967).
[38] A. E. H. Love, *A Treatise on the Mathematical Theory of Elasticity* (Dover, New York, 1944).
[39] R. Granek, J. Phys. II **7**, 1761 (1997).
[40] D. Forster, *Hydrodynamic Fluctuations, Broken Symmetry and Correlation Function* (Addison Wesley, Reading, MA, 1983).
[41] F. C. MacKintosh, J. Käs, and P. A. Janmey, Phys. Rev. Lett. **75**, 4425 (1995).
[42] C. F. Schmidt *et al.*, Macromolecules **22**, 3638 (1989).
[43] D. Needham and E. Evans, Biochemistry **27**, 8261 (1988).
[44] R. Dimova, B. Pouligny, and C. Dietrich, Biophys. J. **79**, 340 (2000).